Comparative ROI analysis for Traumatic Brain Injury with TBSS and XTRACT masks using DTI and NODDI models

by

Maria Baida

THESIS

Submitted in partial satisfaction of the requirements for degree of

MASTER OF SCIENCE

in

Biomedical Imaging

in the

GRADUATE DIVISION

of the

UNIVERSITY OF CALIFORNIA, SAN FRANCISCO

Approved:

DocuSigned by:
Pratik Mukherjee
989635ABB72444C...

Pratik Mukherjee

Chair

DocuSigned by:
Alastair Martin

Alastair Martin

DocuSigned by:
Srikantan Nagarajan

Srikantan Nagarajan

DocuSigned by:
Ashish Raj
13BDA73A066E4E0...

Ashish Raj

Committee Members

Acknowledgments

This year I had the honor of completing a thesis project for MSBI, and for this, I am thankful to many people.

First and foremost, I would like to thank my advisor, Dr. Pratik Mukherjee, for providing me the opportunity to complete this wonderful project and contribute to the scientific community. His guidance and immense knowledge helped me in all the time of research writing of this thesis.

Besides my advisor, I would like to thank the rest of my thesis committee: Dr. Alastair Martin, Dr. Srikantan Nagarajan, and Dr. Ashish Raj, for providing support and advice throughout this process. I also thank Dr. Yan Li for her assistance and expertise. Additionally, I am very thankful to the postdoctoral fellow I worked with, Dr. Lanya Cai, for her patience, enthusiasm, and continuous guidance throughout my thesis project. I am highly honored to have learned from and worked alongside such incredible individuals at UCSF.

The MSBI program has been an adventure from start to finish, and my colleagues in the program have made it so. I thank all the MSBI instructors and lecturers for their imparted knowledge as well. Additionally, I am very thankful to the MSBI administrator and directors: Rukayah Abdolcader, Dr. Alastair Martin, and Dr. Susan Noworolski, for I would not be at UCSF in the first place if not for them.

Last but not least, I would like to thank my friends and family, who encouraged and supported me every step of the way. None of this would have been possible without them motivating me to be the best person I can be.

Comparative ROI analysis for Traumatic Brain Injury with TBSS and XTRACT masks using DTI and NODDI models

Maria Baida

Abstract

Traumatic Brain Injury (TBI) is a leading cause of death and disability around the globe. Diffusion tensor imaging (DTI) parameters have been the most commonly used metrics to characterize white matter (WM) microstructures to identify pathology after TBI. More recently, novel metrics like neurite orientation dispersion and density imaging (NODDI) metrics based on multi-shell sequences have provided additional insights to understand WM microstructures. Together with DTI, these metrics predict both short- and long-term impacts of mild TBI (mTBI) on various neural functions, helping to advance mTBI management and treatment. Lateralization analysis based on DTI parameters has also been used to assess neural functions in TBI. When looking at specific brain regions, the region of interest (ROI) analysis based on tract-based spatial statistics (TBSS) with standard space (e.g.,

mapping the JHU atlas to MNI152 standard T1 space) has been widely applied to study mTBI. However, it is facing significant challenges to study moderate-to-severe TBI due to registration difficulties. Registration challenges come from deformation and lesions in those patients. Lately developed ROI analysis methods based on probabilistic tractography (e.g., FSL XTRACT toolbox) in an individual native diffusion space give promises to fill the gap, but the exact advantages and disadvantages compared to using a standard space have not been well documented. In the present study, the ROI analysis on DTI and NODDI parameters was performed on dMRI of 106 patients (PT), 18 friend controls (FC), and 18 orthopedic controls (OC) collected from two time points, using both standard-space method ("TBSS ROI analysis") and native-space method ("XTRACT ROI analysis"). The test-retest reliability of these two methods was compared by evaluating the coefficient of variation (C_V) at each time point, the Pearson's correlation (R) between the two time points, the intra-class correlation coefficient (ICC) between the two time points, and lateralization index at each time point. With these statistics, the aim was to determine the precision of the TBSS ROI analysis and the XTRACT ROI analysis quantitatively in the practice of analyzing a particular dataset. ROI analysis based on a standard atlas mapped to skeletonized tracts showed excellent precision and reproducibility, although some regions exhibited site and scanner differences; ROI analysis based on probabilistic tractography in individual diffusion space showed great potentials to classify patients and controls, but with more variability, encouraging further development and exploration of the pipeline to improve precision and reliability. These results could provide a new and general reference for choosing analysis methods in future dMRI studies.

Contents

List of Figures

List of Tables

Chapter 1

Introduction

Diffusion tensor imaging (DTI) and neurite orientation dispersion and density imaging (NODDI) have been used to characterize white matter (WM) microstructures and to identify pathology after mild traumatic brain injury (mTBI)[1,2]. Palacios et al. (2020) used DTI and NODDI parameters to predict both short- and long-term impacts of mTBI on various neural functions, helping to advance mTBI management and treatment[1]. Due to the growing impacts of TBI on public health worldwide[3,4], it's important to continue this line of work.

In this project, two-shell diffusion MRI data of 106 patients (PT), 18 friend controls (FC), and 18 orthopedic controls (OC) from the TRACK-TBI study (Transforming Research and Clinical Knowledge in Traumatic Brain Injury)[5] were analyzed using DTI and NODDI models, with a specific focus on comparing two alternative methods for Regions of Interest (ROI) analysis. The tract-based spatial statistics (TBSS)[6] WM ROI analysis has been widely used in previous studies[1]. One significant limitation is that the standard space does not always capture individual variability in microstructures, especially in measuring pathological changes. Recent advancement in probabilistic tractography provides a direction of alternative methods for individualized measures of WM tracts. In particular, the XTRACT package

developed by the FSL team is one of the latest pipelines for probabilistic tractography[7]. It enables efficient estimation of an individual's tractography in the native space. It has great potential in studying TBI, because patients exhibit a wide range of structural and functional changes that might not always be detected if being studied by using a standard space template. The advantages and disadvantages compared to using a standard space have not been well documented.

In addition to DTI and NODDI parametrics this study also looks at lateralization index that evaluates the difference between left and right part of the brain. According to the previous works[8–10], it's known that lateralization index is commonly measured in DTI studies. Thus it is important to evaluate lateralization metrics in the two pipelines that are tested in this project.

This study aims to compare these two methods by: (1) measuring the variability of ROI analysis results to infer the precision of each method; (2) assessing the test-retest reproducibility to estimate the reliability of each method[11,12]. The hypothesis of this project was that the two methods will not lead to different conclusions regarding DTI and NODDI differences between patients and controls. However, TBSS ROI analysis results are expected to show greater precision and reliability, while XTRACT ROI analysis pipeline is expected to show greater inter-subject variability.

Chapter 2

Methods

2.1 Participants and image acquisition

In this study a subset of the multi-site collaboration database of the TRACK-TBI project was analyzed[5]. This subset contains 106 patients (PT), 18 friend controls (FC), and 18 orthopedic controls (OC) from 4 different sites, detailed in Table 2.1. Whole-brain diffusion MRI and T1 were collected from each subject at two time points approximately 6 months apart. Diffusion MRI was performed with multi-slice single-shot spin-echo echo-planar pulse sequence, acquired at b = 1000 (echo time = 94 ms; repetition time = 2900 ms) and 3000 s·mm^{-2} (echo time = 122 ms; repetition time = 3500 ms), both for 64 diffusion-encoding directions (slice thickness = 2.4 mm; slice gap= 0 mm; matrix= 96 × 96; FOV = 230 mm). Separate b = 0 s·mm^{-2} volumes were acquired in the reversed phase-encoding direction for each diffusion shell with corresponding acquisition parameters to be used for susceptibility distortion correction. Sagittal three-dimensional (3D) inversion recovery fast spoiled gradient-recalled echo T1-weighted images were acquired with 256-mm FOV and 200 contiguous partitions (1.2 mm) at 256 × 256 matrix.

Table 2.1: Basic information of database in the current study by site.

Site	# of subjects	Scanner model
Baylor College of Medicine	53	Siemens Trio
Harvard Medical School/Massachusetts General Hospital	15	Siemens Skyra
University of California San Francisco	52	Siemens Skyra
Froedtert and Medical College of Wisconsin	22	GE MR750

2.2 DTI processing

The FMRIB Software Library (FSL) version 6.0.2 (Oxford, UK) was used for image processing and DTI parameters computation. Susceptibility induced distortions were corrected using FSL's topup[13] on each diffusion shell. FSL's Eddy[14] command was used on the diffusion data to correct for motion and eddy current distortions, skull stripping, outlier replacement[15], susceptibility-by-movement [16] and slice-to-volume[17] correction. For each subject, eddy current correction was run once on the individual b1000 shell and once with concatenated b1000 and b3000 multi-shell data. The Diffusion Toolbox (dtifit) in FSL was used on the individually processed b1000 data to calculate fractional anisotropy (FA), which represents the integrity of white matter tracts, and mean diffusivity (MD), which describes the average mobility of water molecules. Multi-shell processed data were normalized to their corresponding b0 image to account for differences in echo time. This normalized multi-shell data were used to quantify NODDI parameters with the Accelerated Microstructure Imaging via Convex Optimization (AMICO) Toolbox[18]. The NODDI parameters that were quantified include: the neurite density index (NDI), which infers the strength of neurite connections, orientation dispersion index (ODI), which reflects the spatial configuration of the neurite structures and free water fraction (FISO), which captures the volume of free water in tissue at the microstructural level.

2.3 TBSS analysis

A voxel-wise tract-based spatial statistics (TBSS) were performed on the FA map using FSL's TBSS package for each site. The FA maps at both time points for each subject in the site were registered to the FMRIB58 FA template in MNI152 standard space. The MNI152 standard-space T1-weighted average structural template image was derived from nonlinear registration and averaging of 152 structural images into a common coordinate[19]. Each FA map was transformed by combining the non-linear transform to the target FA image and the affine transform from the determined target image to MNI152 space. The registered FA maps were then averaged and thinned to generate a mean FA skeleton to represent the center of all white matter tracts. The FA white matter skeleton was thresholded to FA > 0.2 to exclude voxels containing gray matter and partial volume effects. Each subject's FA data at both time points were projected onto this mean skeleton to get individual skeletonized FA maps. The voxels within the skeleton were values from the nearest relevant tract center by searching perpendicular to the local skeleton structure for the maximum value in the FA image of the subject. Each subject's FA, MD, NDI, ODI, and FISO maps were then registered and projected onto the white matter skeleton. White matter tract masks were obtained by mapping the Johns Hopkins University (JHU) ICBM-DTI-81 White-Matter Labeled Atlas[20] regions to the white matter skeleton in MNI152[19] space and resampled to 1-mm resolution. Regional values represented by the average voxel value within the selected JHU white matter tract masks were computed for each subject at both time points across all generated DTI and NODDI parameter maps.

2.4 XTRACT processing and analysis

XTRACT is a newly developed FSL software package with a library of standardized tractography protocols to automatically derive and extract individualized white matter tracts in a subject's native space. Prior to running XTRACT, the data for each time point per subject were prepared following FSL's FMRIB's Diffusion Toolbox (FDT) pipeline which included: (1) brain extraction using the Brain Extraction Tool (BET); (2) fitting the probabilistic crossing fiber model using Bayesian Estimation of Diffusion Parameters Obtained using Sampling Techniques (BEDPOSTX) on eddy corrected multi-shell diffusion data; and (3) linear (FLIRT) and non-linear (FNIRT) registration of diffusion space (first b0 volume of multi-shell data after BET) and structural space (T1 after BET) to standard MNI152 space at 1mm resolution. XTRACT loops through a list of predetermined seeds and corresponding termination criteria warped from standard space to the subject's native space and uses probabilistic tractography (PROBTRACKX2) to define subject specific white matter tracts. Tract masks were generated with XTRACT and XTRACT-STATS and used to estimate DTI and NODDI parameter summary statistics including voxel average from within each masked region, thresholded at 0.1 percent.

2.5 Analysis of regional values

From the above pipelines, for each subject regional values for 5 parameters (FA and MD from DTI, NDI, ODI, and FISO from NODDI) were computed from both time points. Among default TBSS and XTRACT regions, 11 out of 48 TBSS regions and 15 out of 42 XTRACT regions were selected for the current study. The selected regions are shown in table 2.2.

These regions were selected for their anatomical correspondence in both ROI analysis pipelines, so that the two pipelines can be directly compared. The comparability of selected

Table 2.2: List of regions in TBSS and XTRACT methods selected for the current study.

White Matter Tract	TBSS regions (11)	XTRACT regions (15)
Corticospinal Tract	CST – L, CST-R	cst-l, cst-r
Superior Longitudinal Fasciculus	SLF-L, SLF-R	slf1-l, slf1-r, slf2-l, slf2-r, slf3-l, slf3-r
Uncinate Fasciculus	UNC-L, UNC-R	uf-l, uf-r
Genu Of Corpus Callosum/ Forceps Minor	GCC	fmi
Splenium Of Corpus Callosum/ Forceps Major	SCC	fma
The Cingulate Gyrus/ Dorsal Cingulum	CGC-L, CGC-R	cbd-l, cbd-r
Middle Cerebellar Peduncle	MCP	mcp

regions might not always be obvious from labeled names. Specifically, superior longitudinal fasciculus (SLF) was measured bilaterally as one region in the TBSS pipeline, but as 3 separate components in the XTRACT pipeline. The uncinate fasciculus was labeled as "UNC" in the TBSS method but "uf" in the XTRACT method. The genu of corpus callosum (GCC) is comparable to the forceps minor ("fmi"), while the splenium of corpus callosum (SCC) is comparable to the forceps major ("fma"). The cingulum - cingulate gyrus (CGC) is comparable to the dorsal cingulum ("cbd"). The regions known to be easily confounded (e.g., fornix regions are easily partial volume averaged with cerebrospinal fluid) were excluded. Some of these regions form pairs of bilaterally measured regions.

The comparative analysis was focused on test-retest reliability by computing the coefficient of variation (C_V) of each region at each time point across all subjects, the Pearson's correlation (R) between the two time points, and the intra-class correlation coefficient (ICC) between the two time points. The C_V is computed as the ratio of standard deviation and mean, which is the reciprocal of signal-to-noise ratio. In a given comparison, a distribution of regional values with lower C_V has lower variability, therefore indicating a higher precision in the estimation method. Pearson's correlation and intra-class correlation indicate to what extent regional values from the first test were replicated by its counterpart from the second test, with slightly different assumptions on pooling the total variability. The criterion for

Pearson's correlation is that the probability of null hypothesis ($R = 0$) is lower than 0.05. The criterion for intra-class correlation is that ICC > 0.6 is considered a good test-retest reliability.

Finally, the lateralization index was computed by using the equation: $(R-L)\cdot(R+L)^{-1}$, where R and L denote the right and left values in a bilateral pair, respectively.

Chapter 3

Results

The analyses described in the Methods section were successfully performed both for control subjects and patients using both TBSS and XTRACT pipelines. Figure 3.1 shows an example of TBSS pipeline results for skeletonized FA for one subject from the first site at the first time point overlapping with mean FA map from the first site visualized with FSLeyes. The analyses of the TBSS pipeline and XTRACT pipeline achieved results that were different in a variety of ways. These differences are visualized and described in the following paragraphs.

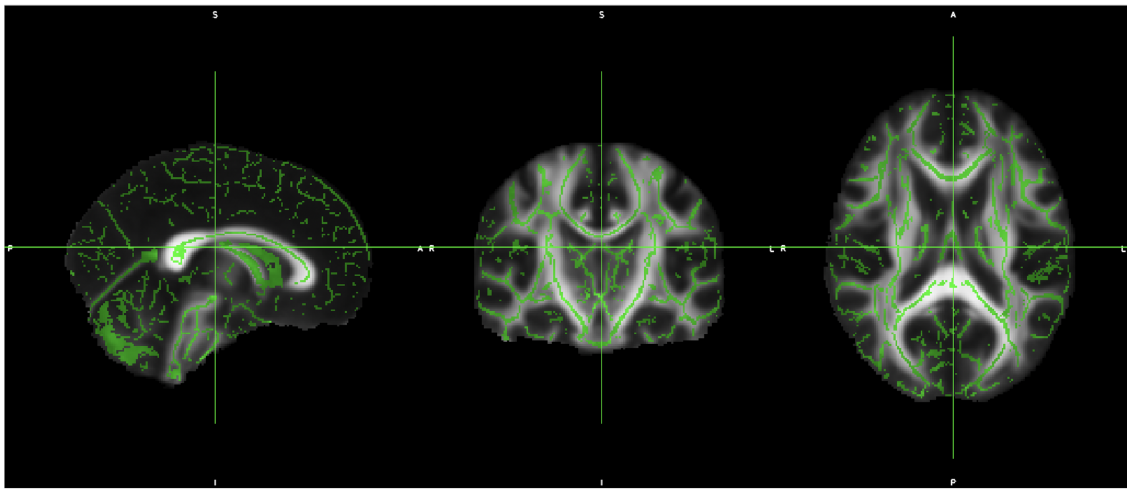

Figure 3.1: TBSS method results for skeletonized FA for one subject from the first site at the first time point overlapping with mean FA map from the first site.

First, a direct visualization of regional values by scatter plots will be shown. Figure 3.2 shows an example of the regional values of the DTI parameter FA in two regions (SCC from TBSS and fma from XTRACT). Blue, red, and yellow markers are data from FC, OC, and PT, respectively. In each cluster of markers, 4 shapes of markers are used to distinguish between sites (circles for the first site, triangles for the second site, squares for the third site, and pentagons for the fourth site). In this figure, the FA values from the TBSS pipeline were higher and less variable across sites and subjects than the FA values from the XTRACT pipeline. Also, the XTRACT pipeline gave fewer successful estimates as the number of markers is visibly smaller (especially for FC), whereas the TBSS pipeline had no miss in estimation.

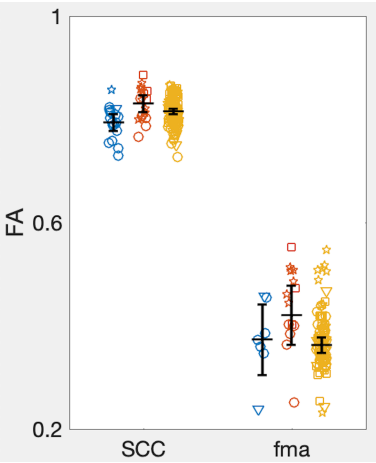

Figure 3.2: The FA values of "SCC" and "fma" from ROI analysis from the first time point from all sites in all subjects - friend controls (blue), orthopedic controls (red), and patients (yellow). Four marker shapes are used to distinguish between sites.

Then, figure 3.3 shows the regional values of DTI and NODDI parameters in the selected 26 regions that are comparable across both TBSS and XTRACT methods and were shown in the table 2.2, are labeled at the bottom of the figure. The uppercase names are regions from the TBSS method, and the lowercase names are regions from the XTRACT. Anatomically comparable regions from the two pipelines are shown in adjacency. The results shown in this figure are from the first time point in all subjects from all sites. For each region from each cohort, the mean and the 95% confidence interval for mean estimation are indicated by black

error bars. For a region of a cohort with no greater than 5 successfully estimated subjects, no confidence intervals can be estimated, there only an algebraic average is computed and indicated as a black bar. Differences between PT and FC and between PT and OC are characterized by two-sample t-tests. A red star on the x-axis indicates a significant difference ($p < 0.05$), whereas a black small dot on the x-axis indicates a non-significant difference.

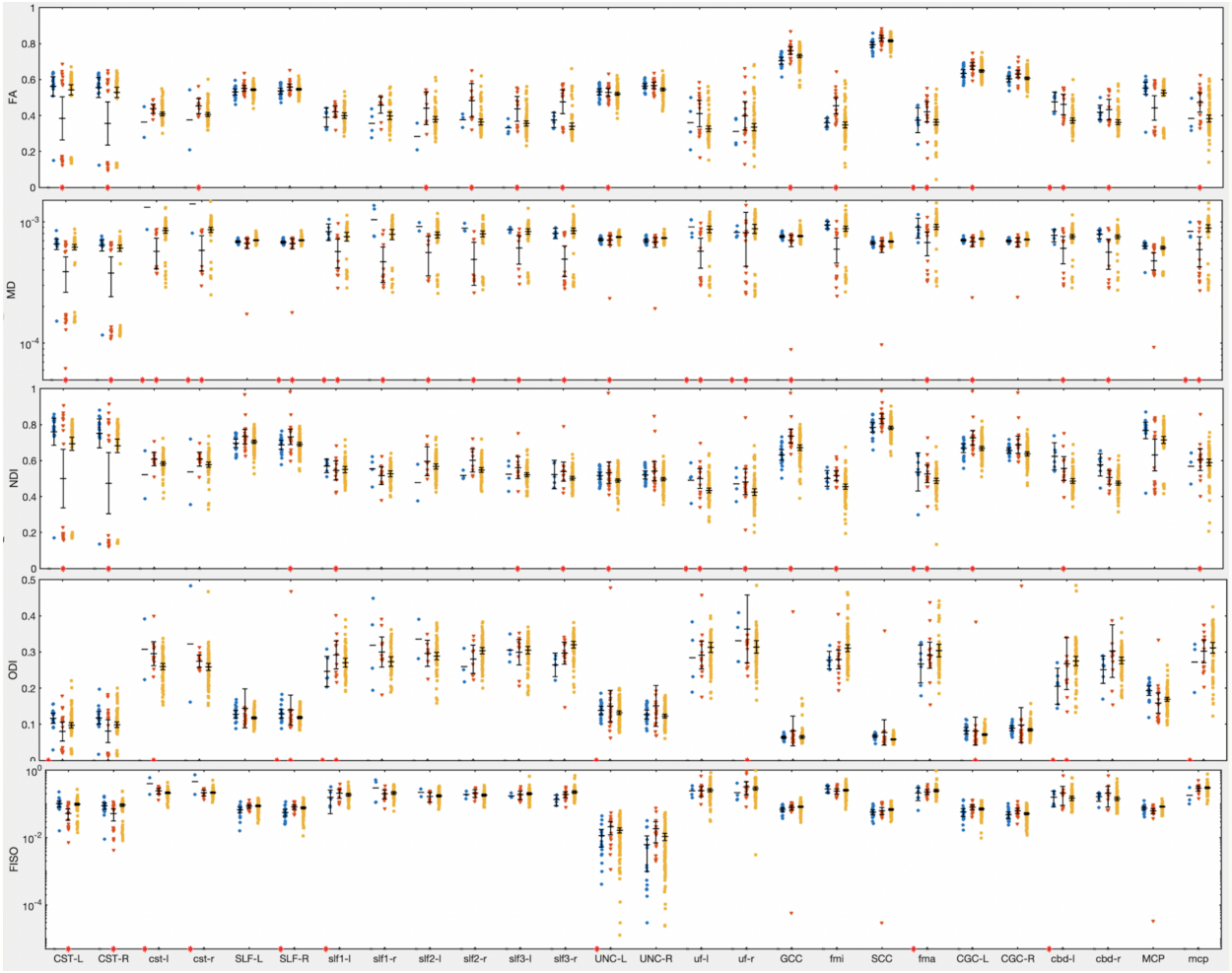

Figure 3.3: Regional values from ROI analysis on DTI parameters (the top panel for FA, and the 2nd panel for MD) and NODDI parameters (the 3rd to 5th panels for NDI, ODI, and FISO, respectively) from the first time point from all sites in all subjects - friend controls (blue), orthopedic controls (red), and patients (yellow).

Importantly, even though the selected regions are considered closely relevant, it is worth mentioning that regional values from the TBSS pipeline are based on skeletonized 2D segments of tracts, whereas the counterparts from XTRACT are based on estimated 3D whole-tracts. This fundamental difference between the two methods may underline any systematic

patterns exhibited in Figure 3.3, qualitatively summarized here: (1) regional values of FA and NDI from the TBSS pipeline are higher than counterparts from the XTRACT pipeline; (2) regional values of MD, ODI, and FISO from the TBSS pipeline are lower than counterparts from the XTRACT pipeline; (3) regional values from the XTRACT pipeline are more variable across subjects than counterparts from the TBSS pipeline; (4) most groups of data are well characterized by a unimodal distribution, although there are exceptions, for instance, the TBSS regions CST-L, CST-R, MCP might have bimodal distributions in FA and NDI values, which can be attributed to site and scanner differences. All the values in the lower group of bimodal distribution were obtained from the same site, which indicates that registration from this site for these regions was different in this site comparing to the other sites. In most of the XTRACT regions, the larger error bars were seen, especially from the OC and FC groups. The larger error bars can be attributed to the smaller number of subjects available for computation of this distribution of these cohorts.

Differences between PT and FC and between PT and OC are characterized by two-sample t-tests. A red star on the x-axis on the figure 3.3 indicates a significant difference. For FA, there are 5 TBSS regions and 10 from XTRACT regions that showed significant differences between PT and control cohorts. For MD, there are 6 TBSS regions and 14 XTRACT regions that showed significant differences between PT and control cohorts.For NDI, there are 6 TBSS regions and 9 XTRACT regions that showed significant differences between PT and control cohorts. For ODI, there are 4 TBSS regions and 5 XTRACT regions that showed significant differences between PT and control cohorts. For FA, there are 4 TBSS regions and 5 XTRACT regions that showed significant differences between PT and control cohorts. This is a qualitative summary. Exact interpretations need future investigation.

To analyze these differences quantitatively, the coefficient of variation of these regions was computed. The results are shown in Figure 3.4. The layout of Figure 3.4 is consistent with Figure 3.3. Regions are labeled on the bottom of the 5th panel. Blue, red, and yellow

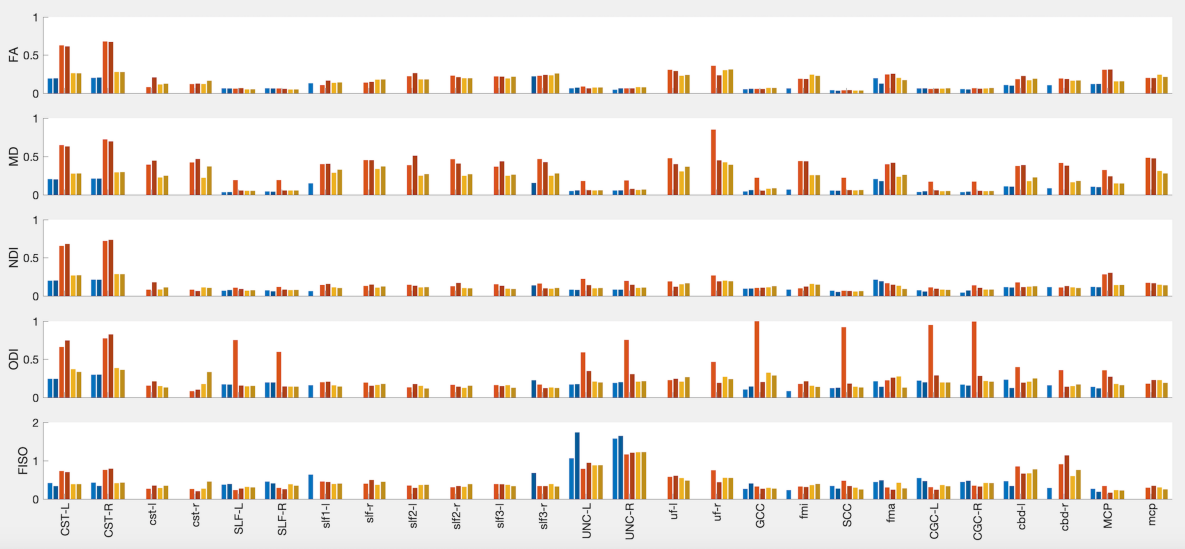

Figure 3.4: Coefficient of variation of regional values.

bars show C_V values for FC, OC, and PT from the first and second tests, respectively. From the first test, TBSS regions have significantly higher C_V NDI ($t(24) = 2.56$, $p = 0.017$), ODI ($t(24) = 4.21$, $p < 0.001$, and FISO ($t(24) = 3.47$, $p = 0.002$, and marginally higher FA ($t(24) = 1.94$, $p = 0.06$), but not MD. Consistently from the second test, these differences are also significant ($t(24) = 2.41$, $p = 0.02$ for FA, $t(24) = 2.13$, $p = 0.04$ for MD, $t(24) = 3.00$, $p = 0.006$ for NDI, $t(24) = 4.21$, $p < 0.001$ for ODI, $t(24) = 3.28$, $p = 0.003$ for FISO.

Figure 3.4 showed that the CV comparison between the TBSS pipeline outcomes and the XTRACT pipeline outcomes depends on regions. Specifically, "CST" had higher CV values than "cst" for all parameters, but otherwise most TBSS regions had lower CV values than their XTRACT counterparts for FA and MD. It is also noticeable that many bars with a relatively high CV correspond to a non-unimodal distribution from Figure 3.3, possibly due to site and scanner differences. Taken together, the CV comparison of the two methods is not conclusive. Formal mathematical decision on excluding or clustering criteria of capturing the site difference is necessary, but beyond the scope of the current project.

To measure the test-retest reliability quantitatively, the Pearson's correlation between paired regional values from the two time points was computed. The impact of brain injury

in PT or non-brain injury in OC cannot be ruled out in these evaluations, even if this impact could be minimal. Therefore, the test-retest reliability assessment for this method should rely on FC subjects data. The advantage of the TBSS pipeline in reproducibility is true for the most of the parameters. Table 3.1 reports the statistics of Pearson's correlation for the 5 parameters for FC. Interestingly, none of the XTRACT regions have shown significant values for Pearson's correlation, with exception of fma in MD and FISO parameters. At the same time most of the TBSS regions have shown the significant values for most of the parameters for Pearson's correlation, which indicates excellent reproducibility for TBSS pipeline.

Table 3.1: Test-retest reliability: Pearson's correlation between two time points for friend controls (FC).

Region	FA	MD	NDI	ODI	FISO
CST-L	R=0.98, p≪0.001	R=0.96, p≪0.001	R=0.98, p≪0.001	R=0.96, p≪0.001	R=0.77, p≪0.001
CST-R	R=0.97, p≪0.001	R=0.97, p≪0.001	R=0.96, p≪0.001	R=0.96, p≪0.001	R=0.88, p≪0.001
cst-l					
cst-r					
SLF-L	R=0.94, p≪0.001	R=0.89, p≪0.001	R=0.67, p=0.002	R=0.9, p≪0.001	
SLF-R	R=0.95, p≪0.001	R=0.94, p≪0.001	R=0.69, p=0.001	R=0.97, p≪0.001	R=0.67, p=0.002
slf2-l					
slf2-r					
slf3-l					
slf3-r					
UNC-L	R=0.83, p≪0.001	R=0.64, p=0.004	R=0.92, p≪0.001	R=0.84, p≪0.001	
UNC-R	R=0.62, p=0.006	R=0.87, p≪0.001	R=0.93, p≪0.001	R=0.77, p≪0.001	R=0.6, p=0.019
uf-l					
uf-r					
GCC	R=0.87, p≪0.001	R=0.83, p≪0.001	R=0.73, p≪0.001	R=0.48, p=0.04	
fmi					
SCC	R=0.85, p≪0.001	R=0.81, p≪0.001	R=0.81, p≪0.001	R=0.89, p≪0.001	R=0.5, p=0.037
fma		R=0.95, p=0.014			R=0.94, p=0.016
CGC-L	R=0.89, p≪0.001	R=0.73, p≪0.001	R=0.73, p≪0.001	R=0.78, p≪0.001	R=0.84, p≪0.001
CGC-R	R=0.86, p≪0.001	R=0.67, p=0.002			R=0.56, p=0.017
cbd-l					
cbd-r					
MCP	R=0.96, p≪0.001	R=0.96, p≪0.001	R=0.97, p≪0.001	R=0.95, p≪0.001	R=0.67, p=0.003
mcp					

Next, the intra-class correlation coefficient (ICC) between paired regional values from the two time points was computed. The results are shown in Figure 3.5. Each bar shows the average ICC across subjects. The numbers at the very top show the number of subjects each bar value was averaged from. There was no missing estimate from the TBSS pipeline, therefore the number of subjects for ICCs of TBSS regions is always the total number of subjects (142). In contrast, the XTRACT pipeline has missing estimates depending on the difficulty of tractography for certain tracts. If several subjects missed either time points for a region,

the number of paired data for ICC computation would be limited. With this limitation in mind, the criterion of ICC > 0.6 for "good reproducibility" was used, marked as the dash line on each panel in Figure 3.5. Bars meeting this criterion are marked with a black star. Across all panels, most TBSS regions (except FISO for GCC, and ODI and FISO for MCP) show good reproducibility between the two time points, suggesting trustable precision and reliability of the method. XTRACT regions do not show reproducibility as much, suggesting that the method is less stable in measuring regional values of DTI and NODDI parameters, although NDI in many XTRACT regions were robustly measured. These results are coherent with Pearson's correlation results. The meaning of the correlation in the PT cohort between the 2 time points, has to be treated differently from FC and OC cohorts, because it has 2 components: besides showing the correlation between 2 repeated measurements, it could also show a potential pathological change between the 2 time points.

Next, the lateralization index was computed for 5 pairs of regions that were bilaterally measured. Figure 3.6 shows the lateralization index at 2-week time point for all parameters from all sites in all subjects - friend controls (blue), orthopedic controls (red), and patients (yellow). Lateralization index is defined as $(R - L) \cdot (R + L)^{-1}$, where R and L denote the right and left values in a bilateral pair, respectively. Therefore, the positive value for lateralization index indicates right-lateralization, which is marked on figure 3.6 by red error-bars, and the negative value indicates left-lateralization, marked by blue. In general, the results replicated findings reported in the literature. For example, the FA values of CGC and CST are left-lateralized[8,9,21]. It can also be seen that UNC is right lateralized, but UNC has been reported with varied lateralization[10,21]. XTRACT regions are qualitatively consistent with TBSS regions, although with exceptions.

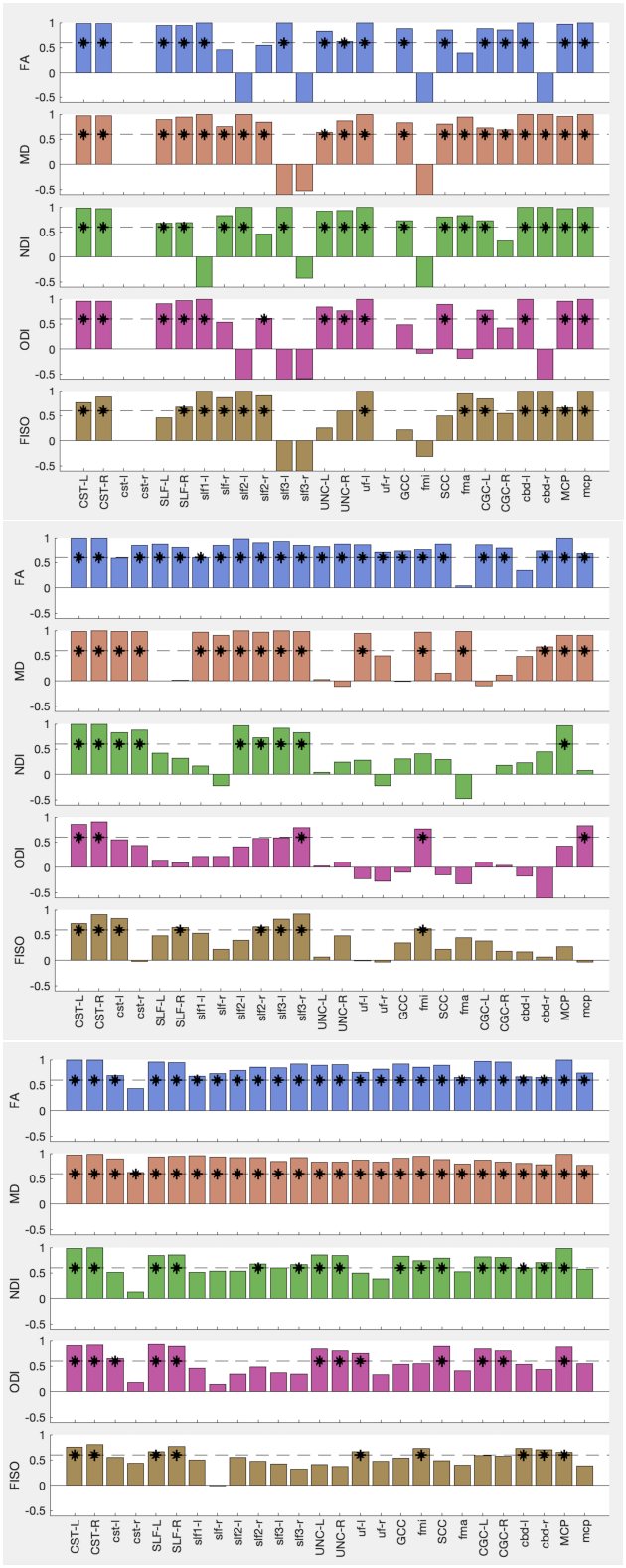

Figure 3.5: Intraclass correlation coefficients between paired regional values from the two time points for FC (the top group of 5 panels), OC (the middle group of 5 panels), and PT (the bottom group of 5 panels).

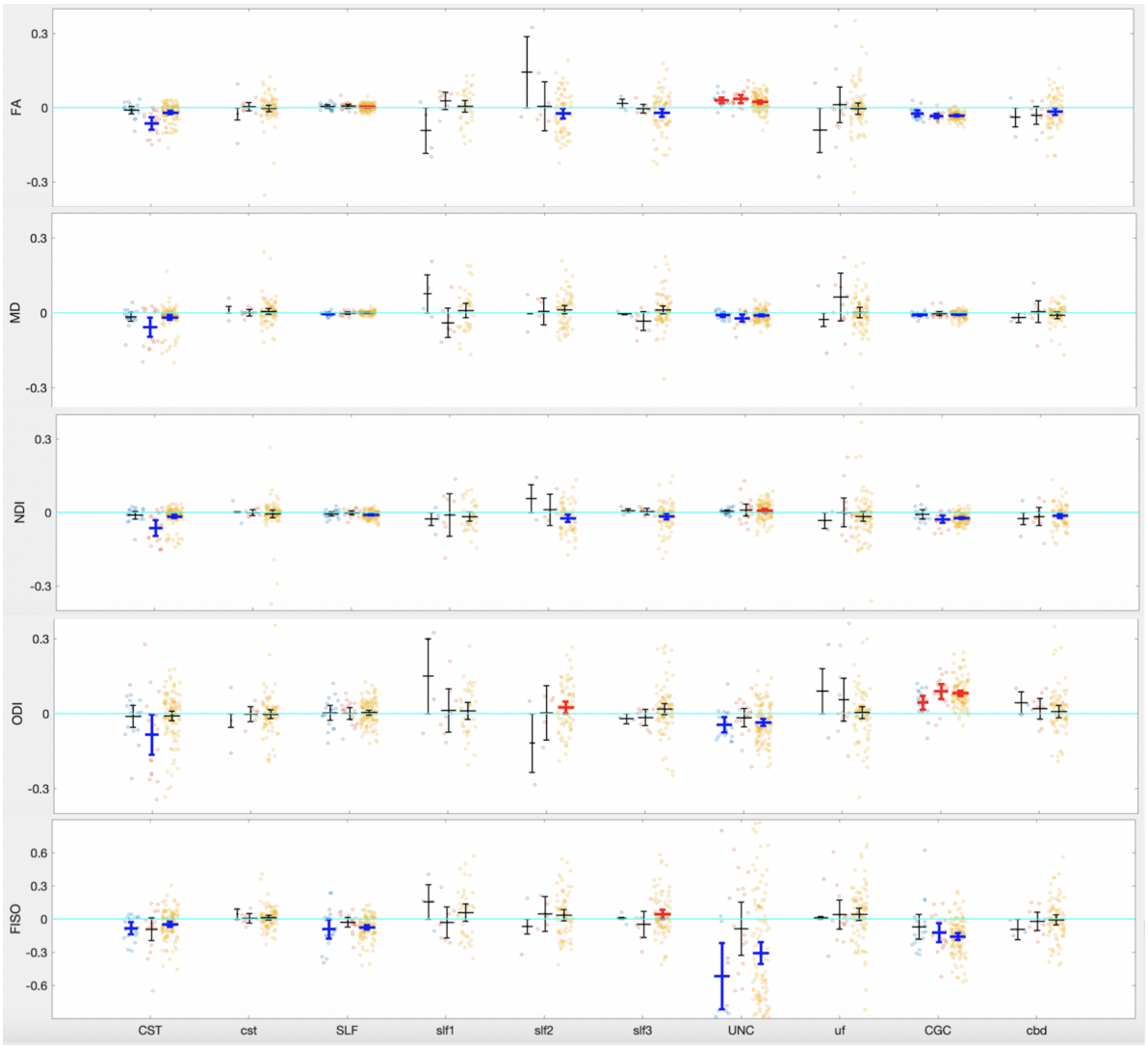

Figure 3.6: Lateralization index of regional values for the first timepoint for all parameters from all sites in all subjects.

Chapter 4

Discussion

In this project, the potential of performing ROI analysis of DTI and NODDI parameters in individual native diffusion space with probabilistic tractography was explored. In reference to the ROI analysis based on probabilistic tractography in individual diffusion space, the ROI analysis based on a standard atlas mapped to skeletonized tracts showed great precision with high test-retest reliability between the two time points in the analyzed dataset. The XTRACT pipeline showed significant reproducibility in many analyzed regions, but with more variability.

A few instances of data patterns not meeting the expectations were found. In Figure 3.3, a bimodal distribution would have characterized the variability better in CST and MCP for FA, MD, and NDI, than the currently assumed unimodal distribution with Gaussian errorbars. The lower cluster of each mentioned region consisting of all data from one out of the four sites was identified, suggesting that the bimodal pattern coincides with site and scanner differences. These differences seem to also show up in Figure 3.4 as the bimodal variability led to increased Cv values in both TBSS and XTRACT regions. These patterns bring up an issue: the cross-sectional analysis between cohorts using t-test becomes confounded, because

t-test has a parametric assumption that does not hold for bimodal distributions. To improve the cross-sectional analysis, harmonization across data from different sites and scanners is necessary. Together with the lateralization evaluation results, the clinical interpretation of these difference reported in the current study need further investigations.

Among DTI and NODDI parameters, NDI regional values were relatively robust to pipeline choice, suggesting that it is a stable metric for characterizing white matter microstructure. The NDI robustness could be explained by the following fact. In reference to the DTI parameters, one advantage of the NODDI parameters is that the free water component is distinguished from neurite density estimation, which makes the measurement of tract regional values of NDI resistant to contamination from the cerebrospinal fluid. In general, the results show lower FA, higher MD, and more variation of regional values from tractography based pipeline than the counterparts from the TBSS pipeline. These differences might be partially attributed to the fact that 3D tract masks are more likely to include peripheral (non-core) and termination (non-central) zones, and possibly cerebrospinal fluid, whereas the multi-slice 2D TBSS masks and therefore regional values were estimated from the skeletonized core of the central part of each tract.

Understanding the nature of probabilistic tractography as a source of analysis result variability is conforming to the pursuit of reproducibility. Theaud et al. (2020) mentioned that software stability and random seed generation for tractography should be carefully considered and tested in assessment of pipeline reproducibility. Additionally, fiber tracking was constructed as a stochastic process, which by nature will result in non-deterministic track segments, although one could usually make assumptions to model the distribution [22].

The sources of variability in the XTRACT pipeline should be carefully considered. Due to the fact that individual native space was used for the XTRACT method, the inter-subject variability is expected. This can be a desirable advantage of the current pipeline because it is capable of showing unique individual specificity in white matter microstructure. However,

the intra-subject variability calls into question the measurement of the precision of this method. To reduce intra-subject variability and improve the precision in the XTRACT pipeline, the following strategies could be considered to be further tested: (1) use FreeSurfer to reconstruct the cortical surface from the individual's T1 image volume, and use the surface instead of using a standard T1 template as a seeding reference for tractography; (2) use a "zeppelin" model instead of a "ball-stick" model for fibres to obtain Bayesian estimation of the crossing fibres density map, especially when high quality of dMRI data is available.

Chapter 5

Conclusion

Region-of-interest analysis of diffusion MRI metrics based on tract-based spatial statistics, which was widely used to study mTBI, is facing significant challenges to study moderate-to-severe TBI due to deformation and lesions in those patients. Precise and reproducible region segmentation based on advanced tractography, with the expectation to show individual specificity gives promises to fill that gap. In the current study, 2D tract skeleton TBSS ROI analysis based on a standard atlas mapped to skeletonized tracts exhibited excellent precision and reproducibility; 3D whole-tract XTRACT ROI analysis based on probabilistic tractography in individual diffusion space showed great potentials to classify patients and controls, but with more variability, encouraging further development and exploration of the pipeline to improve reliability and precision. Despite the findings reported in the literature, that suggest that NODDI metrics might have more cross-scanner variability than DTI metrics, especially when there are differences in the dMRI sequence such as single-band versus multi-band echoplanar imaging[1,23–25], neurite density index was relatively robust to pipeline choice, suggesting that it is a stable metric for characterizing WM microstructure.

Bibliography

[1] Eva M Palacios, Julia P Owen, Esther L Yuh, Maxwell B Wang, Mary J Vassar, Adam R Ferguson, Ramon Diaz-Arrastia, Joseph T Giacino, David O Okonkwo, Claudia S Robertson, et al. The evolution of white matter microstructural changes after mild traumatic brain injury: a longitudinal dti and noddi study. *Science advances*, 6 (32):eaaz6892, 2020. 1, 21

[2] Esther L Yuh, Shelly R Cooper, Pratik Mukherjee, John K Yue, Hester F Lingsma, Wayne A Gordon, Alex B Valadka, David O Okonkwo, David M Schnyer, Mary J Vassar, et al. Diffusion tensor imaging for outcome prediction in mild traumatic brain injury: a track-tbi study. *Journal of neurotrauma*, 31(17):1457–1477, 2014. 1

[3] Raquel C Gardner and Kristine Yaffe. Epidemiology of mild traumatic brain injury and neurodegenerative disease. *Molecular and Cellular Neuroscience*, 66:75–80, 2015. 1

[4] P Leo and M McCrea. Epidemiology. In Daniel Laskowitz and Gerald Grant, editors, *Translational research in traumatic brain injury*. CRC Press/Taylor and Francis Group, 2016. 1

[5] John K Yue, Mary J Vassar, Hester F Lingsma, Shelly R Cooper, David O Okonkwo, Alex B Valadka, Wayne A Gordon, Andrew IR Maas, Pratik Mukherjee, Esther L Yuh, et al. Transforming research and clinical knowledge in traumatic brain injury pilot:

multicenter implementation of the common data elements for traumatic brain injury. *Journal of neurotrauma*, 30(22):1831–1844, 2013. 1, 3

[6] Stephen M Smith, Mark Jenkinson, Heidi Johansen-Berg, Daniel Rueckert, Thomas E Nichols, Clare E Mackay, Kate E Watkins, Olga Ciccarelli, M Zaheer Cader, Paul M Matthews, et al. Tract-based spatial statistics: voxelwise analysis of multi-subject diffusion data. *Neuroimage*, 31(4):1487–1505, 2006. 1

[7] Shaun Warrington, Katherine L Bryant, Alexandr A Khrapitchev, Jerome Sallet, Marina Charquero-Ballester, Gwenaëlle Douaud, Saad Jbabdi, Rogier B Mars, and Stamatios N Soheairopoulos. Xtract-standardised protocols for automated tractography in the human and macaque brain. *NeuroImage*, 217:116923, 2020. 2

[8] Gaolang Gong, Tianzi Jiang, Chaozhe Zhu, Yufeng Zang, Fei Wang, Sheng Xie, Jiangxi Xiao, and Xuemei Guo. Asymmetry analysis of cingulum based on scale-invariant parameterization by diffusion tensor imaging. *Human brain mapping*, 24(2):92–98, 2005. 2, 15

[9] Judith S Verhoeven, Caroline A Sage, Alexander Leemans, Wim Van Hecke, Dorothée Callaert, Ronald Peeters, Paul De Cock, Lieven Lagae, and Stefan Sunaert. Construction of a stereotaxic dti atlas with full diffusion tensor information for studying white matter maturation from childhood to adolescence using tractography-based segmentations. *Human brain mapping*, 31(3):470–486, 2010. 15

[10] Derek K Jones, Marco Catani, Carlo Pierpaoli, Suzanne JC Reeves, Sukhwinder S Shergill, Michael O'Sullivan, Pasha Golesworthy, Phillip McGuire, Mark A Horsfield, Andrew Simmons, et al. Age effects on diffusion tensor magnetic resonance imaging tractography measures of frontal cortex connections in schizophrenia. *Human brain mapping*, 27(3):230–238, 2006. 2, 15

[11] Garikoitz Lerma-Usabiaga, Pratik Mukherjee, Zhimei Ren, Michael L Perry, and

Brian A Wandell. Replication and generalization in applied neuroimaging. *Neuroimage*, 202:116048, 2019. 2

[12] Garikoitz Lerma-Usabiaga, Pratik Mukherjee, Michael L Perry, and Brian A Wandell. Data-science ready, multisite, human diffusion mri white-matter-tract statistics. *Scientific data*, 7(1):1–9, 2020. 2

[13] Jesper LR Andersson, Stefan Skare, and John Ashburner. How to correct susceptibility distortions in spin-echo echo-planar images: application to diffusion tensor imaging. *Neuroimage*, 20(2):870–888, 2003. 4

[14] Jesper LR Andersson and Stamatios N Sotiropoulos. An integrated approach to correction for off-resonance effects and subject movement in diffusion mr imaging. *Neuroimage*, 125:1063–1078, 2016. 4

[15] Jesper LR Andersson, Mark S Graham, Enikő Zsoldos, and Stamatios N Sotiropoulos. Incorporating outlier detection and replacement into a non-parametric framework for movement and distortion correction of diffusion mr images. *Neuroimage*, 141:556–572, 2016. 4

[16] Jesper LR Andersson, Mark S Graham, Ivana Drobnjak, Hui Zhang, and Jon Campbell. Susceptibility-induced distortion that varies due to motion: Correction in diffusion mr without acquiring additional data. *Neuroimage*, 171:277–295, 2018. 4

[17] Jesper LR Andersson, Mark S Graham, Ivana Drobnjak, Hui Zhang, Nicola Filippini, and Matteo Bastiani. Towards a comprehensive framework for movement and distortion correction of diffusion mr images: Within volume movement. *Neuroimage*, 152:450–466, 2017. 4

[18] Alessandro Daducci, Erick J Canales-Rodríguez, Hui Zhang, Tim B Dyrby, Daniel C Alexander, and Jean-Philippe Thiran. Accelerated microstructure imaging via convex optimization (amico) from diffusion mri data. *NeuroImage*, 105:32–44, 2015. 4

[19] Vladimir S Fonov, Alan C Evans, Robert C McKinstry, CR Almli, and DL Collins. Unbiased nonlinear average age-appropriate brain templates from birth to adulthood. *NeuroImage*, (47):S102, 2009. 5

[20] Kenichi Oishi, Andreia Faria, Hangyi Jiang, Xin Li, Kazi Akhter, Jiangyang Zhang, John T Hsu, Michael I Miller, Peter CM van Zijl, Marilyn Albert, et al. Atlas-based whole brain white matter analysis using large deformation diffeomorphic metric mapping: application to normal elderly and alzheimer's disease participants. *Neuroimage*, 46(2):486–499, 2009. 5

[21] Michel Thiebaut De Schotten, Flavio Dell'Acqua, Stephanie Forkel, Andrew Simmons, Francesco Vergani, Declan GM Murphy, and Marco Catani. A lateralized brain network for visuo-spatial attention. *Nature Precedings*, pages 1–1, 2011. 15

[22] Guillaume Theaud, Jean-Christophe Houde, Arnaud Boré, François Rheault, Felix Morency, and Maxime Descoteaux. Tractoflow: A robust, efficient and reproducible diffusion mri pipeline leveraging nextflow & singularity. *NeuroImage*, 218:116889, 2020. 19

[23] Christina Andica, Koji Kamagata, Takuya Hayashi, Akifumi Hagiwara, Wataru Uchida, Yuya Saito, Kouhei Kamiya, Shohei Fujita, Toshiaki Akashi, Akihiko Wada, et al. Scan–rescan and inter-vendor reproducibility of neurite orientation dispersion and density imaging metrics. *Neuroradiology*, 62(4):483–494, 2020. 21

[24] Samira Bouyagoub, Nicholas G Dowell, Matt Gabel, and Mara Cercignani. Comparing multiband and singleband epi in noddi at 3 t: what are the implications for reproducibility and study sample sizes? *Magnetic Resonance Materials in Physics, Biology and Medicine*, pages 1–13, 2020.

[25] Martina Lucignani, Laura Breschi, Maria Camilla Rossi Espagnet, Daniela Longo, Lorenzo Figà Talamanca, Elisa Placidi, and Antonio Napolitano. Reliability on multi-

band diffusion noddi models: a test retest study on children and adults. *NeuroImage*, page 118234, 2021. 21

Publishing Agreement

It is the policy of the University to encourage open access and broad distribution of all theses, dissertations, and manuscripts. The Graduate Division will facilitate the distribution of UCSF theses, dissertations, and manuscripts to the UCSF Library for open access and distribution. UCSF will make such theses, dissertations, and manuscripts accessible to the public and will take reasonable steps to preserve these works in perpetuity.

I hereby grant the non-exclusive, perpetual right to The Regents of the University of California to reproduce, publicly display, distribute, preserve, and publish copies of my thesis, dissertation, or manuscript in any form or media, now existing or later derived, including access online for teaching, research, and public service purposes.

DocuSigned by:
Maria Baida
C93CFDBCB4D84A7...
Author Signature

9/2/2021
Date